View metadata, citation and similar papers at core.ac.uk

brought to you by CORE

provided by UNT Digital Library

LAWRENCE
LIVERMORE
NATIONAL
LABORATORY

UCRL-SR-228619

Final Report for Time Domain Boundary Element and Hybrid Finite Element Simulation for Maxwell's Equations

James Pingenot, Vikram Jandhyala

March 4, 2007

Disclaimer

This document was prepared as an account of work sponsored by an agency of the United States Government. Neither the United States Government nor the University of California nor any of their employees, makes any warranty, express or implied, or assumes any legal liability or responsibility for the accuracy, completeness, or usefulness of any information, apparatus, product, or process disclosed, or represents that its use would not infringe privately owned rights. Reference herein to any specific commercial product, process, or service by trade name, trademark, manufacturer, or otherwise, does not necessarily constitute or imply its endorsement, recommendation, or favoring by the United States Government or the University of California. The views and opinions of authors expressed herein do not necessarily state or reflect those of the United States Government or the University of California, and shall not be used for advertising or product endorsement purposes.

This work was performed under the auspices of the U.S. Department of Energy by University of California, Lawrence Livermore National Laboratory under Contract W-7405-Eng-48.

Final Report for "Time Domain Boundary Element and Hybrid Finite Element Simulation for Maxwells Equations,"

Lawrence Livermore National Laboratory Subcontract B541344,
University of Washington Reference Number A8733/FA6886

James Pingenot and Vikram Jandhyala

February 22, 2007

Abstract

This report summarizes the work performed for Lawrence Livermore National Laboratory (LLNL) at the University of Washington between September 2004 and May 2006. This project studied fast solvers and stability for time domain integral equations (TDIE), especially as applied to radiating boundary for a massively parallel FEM solver.

1 Introduction

Time-domain integral equations (TDIEs) are now powerful and rapidly evolving tools for temporal simulation of electromagnetic behavior of complex structures. A popular use of TDIEs is as a boundary condition for volume methods such as FDTD and FEM. A small sampling of the literature on this subject can be found here [1–4]. TDIEs provide an extremely accurate boundary condition for volume methods, exactly modeling free space radiation, subject to discretization error. For most cases, the results are much more accurate than those achieved by either absorbing boundary conditions or perfectly matched layers. Furthermore, TDIEs are relatively easy to parallelize, making them amenable for use in massively parallel environments such as Lawrence Livermore National Laboratory (LLNL).

The main problem in using integral equations as radiation boundaries is that they are computationally expensive, scaling as $O(N_t N_s^2)$ in both time and memory, where N_s is the number of spatial unknowns and N_t is the number of time steps. This increased cost is the main reason that the TDIE radiation boundary is not often used. In September of 2003 LLNL contracted with the University of Washington to study the implementation of a fast solver for TDIEs that would be useful for the EMSolve finite element code. The main requirements of this solver were that it be parallelizeable and work for general 3D structures.

In the frequency domain, there are three methods for fast solvers that have been proven successful: Fast Multipole Methods (FMM), FFT acceleration, and QR compression. The following is a brief description of these methods as applied to the time domain, and how they fit in with this project.

1.1 Plane Wave Time Domain

The Fast Multipole Method has been successfully adapted to the time domain as the Plane Wave Time Domain method (PWTD) [5]. This method achieves scaling as $O(N_t N_s log N_s)$ in cost. It achieves this speedup by lumping basis functions together for distant interactions, while still computing nearby interactions exactly. The process of lumping interactions together is extremely complex and requires an angle-dependent projection.

PWTD has been successfully used for radiation boundary conditions [4], and has even been implemented in parallel [6, 7]. However, the method is extremely difficult to parallelize and so was not chosen for this application.

1.2 Adaptive Integral Method

FFT acceleration has been adapted to the time domain as the Time Domain Adaptive Integral Method (AIM) [8, 9]. This method has also been applied to radiation boundary problems [10], and scales well in a parallel environment [11].

At the start of the project, AIM was the method of choice for accelerating the radiation boundary due to its simple parallelization. However, upon further examination it was found that, while possible [10], AIM has limitations in application to radiation boundaries in the time domain. This is due to the need for a uniform projection grid in space on which to compute interactions. In 2D, the method scales as $O(N_t N_s log^2 N_s)$ in complexity, but for general 3D surfaces this becomes $O(N_t N_s^{1.5} log^2 N_s)$. This is because the uniform grid requires many internal points to be placed within the structure where no radiation interactions occur. Memory scales as $O(N_s^2)$ for both cases.

During a meeting in summer of 2005 it was calculated that, even in the most generous case, the $O(N_t N_s^{1.5} log^2 N_s)$ scaling would require over 1 million surface unknowns to be of benefit to the radiation boundary problem. Therefore it was suggested to leave off this method and try other approaches.

1.3 Multilevel QR decomposition

Another method, showing excellent results in the frequency domain, is the Multilevel QR method [12]. This method relies on expressing dense, low rank matrices via a set of QR decompositions. However, in the time domain all matrices are sparse, and therefore the QR technique is not directly applicable. Several attempts were made at the start of the project to develop a mapping from the sparse matrices to a series of dense matrices, however no suitable methods were found (i.e. methods of $O(N_s)$) and this method was abandoned.

1.4 Multigrid Methods

The method settled on for this project is the Multigrid method, pioneered by Brandt [13]. This method is commonly used in finite elements to increase solution speed, but has not seen much use in integral equations for a number of reasons. Multigrid methods are discussed in more detail in later sections.

1.5 Stability

In addition to the solution speed issues, a generalized TDIE solver faces problems with stability. The lack of a generally stable formulation for electromagnetic TDIEs (and the electric field integral equation specifically) has made progress in this field difficult. Stability has been approached by many researchers [14–17], and while improvements have been made, a generally stable TDIE formulation, or at least a set of rules to guarantee stability, have been elusive. Here, a viewpoint of accurate integration was used in order to enhance the stability of the TDIE solver. This is addressed in Section 2.

1.6 Organization

This report is organized as follows: Section 2 discusses TDIEs and the use of polar integration to stabilize them. The application of the multigrid method to TDIEs as a fast solver is discussed in Section 3.

2 Stability and Polar Integration

This section examines stability in TDIEs. It also shows the results of increasing the stability through more accurate integration of the basis functions.

2.1 Introduction

Several researchers have recently developed techniques for enhancing stability. In addition to special basis functions [14–16] and implicit schemes [17], it is imperative to have accurate space-time quadrature schemes. Compared to frequency domain quadrature, TDIE integration has the additional property of requiring exact time delays between each point in a source region and the observer location. The standard approximation to this is multi-point 2D quadrature [18] with analytical singularity extraction [19], while the Duffy method [20], Nyström method [21], the method presented recently by Khayat and Wilton [22], and methods for conformal elements [23] have been used for more exact integration. However, no study to date has examined how the shape of potential interactions affects the stability of the system. It has been assumed that accurate integration of the spatial component (while accounting for delays) will provide accurate temporal resolution. We find this is not so.

This is of particular importance when meshes have been refined, and both electrically large and electrically small elements are present on the same mesh,

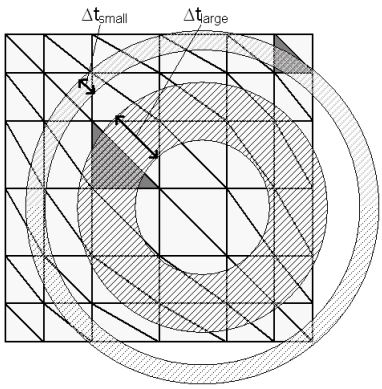

Figure 1: *Mesh of plate, with swept element size. If the time step is chosen as implicit for the large element, important interactions will be missed in the lumping together of small elements. On the other hand, if the integration is not performed exactly, the small time step will be unstable for the larger elements.*

as shown in Figure 1. In this case, a large time step misses important interactions taking place between small elements. However, if the time step is small, the equations for large elements become explicit, leading to instability in the solution. The resolution to this problem is to use a small time step, but to accurately integrate the space-time quadrature of a TDIE system to retain stability for the larger elements.

In this section the exact space integrals for frequency domain vector and scalar potentials developed in [24] are adapted to the space time integrals of the time domain. This method is chosen because it is optimized to accurately predict the temporal shape of potential interactions. The 2D integration of free-space Green's functions are converted to piecewise smooth 1D integrals over delay (with a 1D analytical integration) via a polar transformation, that can easily be addressed by Gauss-Legendre integration. This simple and elegant transformation allows arbitrary accuracy in delay calculations. As shown by the examples, this technique greatly enhances potential accuracy, which may lead to more stable and accurate TDIE codes. The quadrature technique can be applied directly to all integrations: singular, near-singular, close-range, and far-field integrals, arising in different sections of the TDIE matrices. The goal of this section is to show that the delay integration is key to accurate potential calculation. As will be seen in the results, inaccurate potential integration creates spurious high-frequency signals capable of destabilizing TDIE codes. At present this method is limited to planar elements, but may be adapted to conformal elements in the future.

2.2 Formulation

The magnetic vector potential, $\mathbf{A}(\mathbf{r})$, and electric scalar potential, $\phi(\mathbf{r})$, due to a current density, $\mathbf{J}(\mathbf{r},t)$, and charge density, $q(\mathbf{r},t)$, on a surface S, are given by

$$\mathbf{A}(\mathbf{r}) = \frac{\mu}{4\pi}\int_S \frac{\mathbf{J}\left(\mathbf{r}', t-\frac{|\mathbf{r}-\mathbf{r}'|}{c}\right)}{|\mathbf{r}-\mathbf{r}'|}\,ds \tag{1}$$

$$\phi(\mathbf{r}) = \frac{1}{4\pi\epsilon}\int_S \frac{q\left(\mathbf{r}', t-\frac{|\mathbf{r}-\mathbf{r}'|}{c}\right)}{|\mathbf{r}-\mathbf{r}'|}\,ds, \tag{2}$$

where the quantities ϵ, μ, and c are the background material's permittivity, permeability, and propagation velocity, respectively. The current and charge are related by the continuity equation

$$\nabla\cdot\mathbf{J}(\mathbf{r},t) + \dot{q}(\mathbf{r},t) = 0. \tag{3}$$

Following the method used in [14], the current and charge can be written in terms of the same unknown

$$\mathbf{J}(\mathbf{r},t) = \dot{\mathbf{P}}(\mathbf{r},t) \tag{4}$$

$$q(\mathbf{r},t) = -\nabla\cdot\mathbf{P}(\mathbf{r},t). \tag{5}$$

Substituting (4) and (5) into (1) and (2) gives

$$\mathbf{A}(\mathbf{r}) = \frac{\mu}{4\pi}\int_S \frac{\dot{\mathbf{P}}\left(\mathbf{r}', t-\frac{|\mathbf{r}-\mathbf{r}'|}{c}\right)}{|\mathbf{r}-\mathbf{r}'|}\,ds \tag{6}$$

$$\phi(\mathbf{r}) = -\frac{1}{4\pi\epsilon}\int_S \frac{\nabla\cdot\mathbf{P}\left(\mathbf{r}', t-\frac{|\mathbf{r}-\mathbf{r}'|}{c}\right)}{|\mathbf{r}-\mathbf{r}'|}\,ds. \tag{7}$$

The surface is tessellated, and the spatial behavior of the current is characterized by RWG basis functions over adjacent, paired triangles, T^+ and T^-,

$$\mathbf{P}(\mathbf{r},t) = \begin{cases} \frac{l}{2A^\pm}\boldsymbol{\rho}^\pm P(t), & \mathbf{r}\in T^\pm \\ 0, & \mathbf{r}\notin T^\pm \end{cases}, \tag{8}$$

where l is the length of the shared edge between the triangles and $A^\pm$ is the area of the source triangle. The vector $\boldsymbol{\rho}^\pm$ is the vector from (to) the node opposite the shared edge to (from) $\mathbf{r}$ on T^+ (T^-). Figure 2 depicts this basis function. The quantity $P(t)$ characterizes the temporal behavior of $\mathbf{P}(\mathbf{r},t)$. The integration of a basis function over a single triangle can now be described as

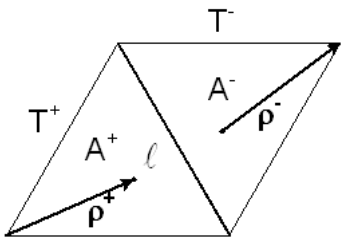

Figure 2: *RWG basis function over two triangles, T^+ and T^-.*

$$\mathbf{A}(\mathbf{r}) = \frac{\mu}{4\pi}\frac{l}{2A^{\pm}}\int_T \frac{\boldsymbol{\rho}^{\pm}\dot{P}\left(t-\frac{|\mathbf{r}-\mathbf{r}'|}{c}\right)}{|\mathbf{r}-\mathbf{r}'|}\,ds \tag{9}$$

$$\phi(\mathbf{r}) = -\frac{1}{4\pi\epsilon}\frac{l}{A^{\pm}}\int_T \frac{P\left(t-\frac{|\mathbf{r}-\mathbf{r}'|}{c}\right)}{|\mathbf{r}-\mathbf{r}'|}\,ds. \tag{10}$$

The key to polar quadrature is taking the surface integration in 3-D space, and transforming it into a 2-D integration in the plane of the source function. The transformation is characterized by

$$\boldsymbol{\rho}^{\pm} = \boldsymbol{\rho} - \boldsymbol{\rho}^c \tag{11}$$

$$R = \sqrt{\rho^2 + d^2} \tag{12}$$

$$ds = \rho\, d\rho\, d\theta, \tag{13}$$

where d is the distance from the observation point to its projection on the plane of the triangle, $\boldsymbol{\rho}$ is the vector from the projection point to the source point, $\boldsymbol{\rho}^c$ is the vector from the projection point to the origin-node of the RWG basis function, and $\rho = |\boldsymbol{\rho}|$. Note that $\boldsymbol{\rho}^c$ is constant with respect to the integration.

The potentials can then be written as

$$\mathbf{A}(\mathbf{r}) = \frac{\mu}{4\pi}\frac{l}{2A^{\pm}}\left[\dot{\mathbf{M}}_{vect} - \boldsymbol{\rho}^c\dot{M}_{scal}\right] \tag{14}$$

$$\phi(\mathbf{r}) = -\frac{1}{4\pi\epsilon}\frac{l}{A^{\pm}}M_{scal}. \tag{15}$$

where

$$\mathbf{M}_{vect} = \iint \frac{\rho^2(\hat{\mathbf{u}}\cos\theta + \hat{\mathbf{v}}\sin\theta)P\left(t - \frac{\sqrt{\rho^2+d^2}}{c}\right)}{\sqrt{\rho^2+d^2}}\, d\rho\, d\theta \tag{16a}$$

$$M_{scal} = \iint \frac{\rho P\left(t - \frac{\sqrt{\rho^2+d^2}}{c}\right)}{\sqrt{\rho^2+d^2}}\, d\rho\, d\theta. \tag{16b}$$

In (16a) the local vector $\boldsymbol{\rho}$ has been broken down into its local Cartesian components as $\boldsymbol{\rho} = \hat{\mathbf{u}}\cos\theta + \hat{\mathbf{v}}\sin\theta$. The temporal derivatives of $P(t)$ in (14) are left for analytical evaluation.

The above integrals can be described by

$$I_{\varphi\chi} = \int_\rho \int_\theta \varphi(\rho)\chi(\theta)\, d\rho\, d\theta. \tag{17}$$

The function φ is defined as either $\varphi_{M,vect}$ or $\varphi_{M,scal}$ where

$$\varphi_{M,vect}(\rho) = \frac{\rho^2 P\left(t - \frac{\sqrt{\rho^2+d^2}}{c}\right)}{\sqrt{\rho^2+d^2}} \tag{18a}$$

$$\varphi_{M,scal}(\rho) = \frac{\rho P\left(t - \frac{\sqrt{\rho^2+d^2}}{c}\right)}{\sqrt{\rho^2+d^2}}. \tag{18b}$$

If $d = 0$ (as in the singular case), these become

$$\varphi_{M,vect}(\rho) = \rho P\left(t - \frac{\rho}{c}\right) \tag{19a}$$

$$\varphi_{M,scal}(\rho) = P\left(t - \frac{\rho}{c}\right), \tag{19b}$$

which is non-singular. The function χ is either $\chi_c = \cos(\theta)$, $\chi_s = \sin(\theta)$ or $\chi_0 = 1$.

Now that the integrand has been separated into functions of the two variables, the integrals may be dealt with separately. The limits of the integration in θ depend on the value of ρ. As illustrated in Figure 3, the circle defined by ρ can intersect a triangle between zero and six places, creating between one and three intervals to analytically integrate in θ. If there are zero intersection points, the interval is $(0, 2\pi)$. We define

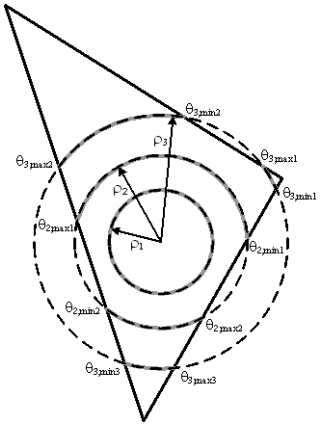

Figure 3: *θ integration regions for three different values of ρ on a triangle.*

$$\begin{aligned}\begin{pmatrix}\xi_c(\rho)\\ \xi_s(\rho)\\ \xi_0(\rho)\end{pmatrix} &= \sum_{i=1}^{K(\rho)} \int_{\theta^i_{min}(\rho)}^{\theta^i_{max}(\rho)} \begin{pmatrix}\cos\theta\\ \sin\theta\\ 1\end{pmatrix}\, d\theta \\ &= \sum_{i=1}^{K(\rho)} \begin{bmatrix}\sin\theta^i_{max}(\rho) - \sin\theta^i_{min}(\rho)\\ -\cos\theta^i_{max}(\rho) + \cos\theta^i_{min}(\rho)\\ \theta^i_{max}(\rho) - \theta^i_{min}(\rho)\end{bmatrix},\end{aligned} \tag{20}$$

where $K(\rho)$ is 1, 2, or 3 depending on ρ. Substituting (18a), (18b), and (20) into (16b) and (16a) gives

$$\mathbf{M}_{vect} = \int_{\rho_{min}}^{\rho_{max}} \varphi_{M,vect}(\rho)\left[\hat{\mathbf{u}}\xi_c(\rho) + \hat{\mathbf{v}}\xi_s(\rho)\right]\, d\rho \tag{21a}$$

$$M_{scal} = \int_{\rho_{min}}^{\rho_{max}} \varphi_{M,scal}(\rho)\xi_0(\rho)\, d\rho. \tag{21b}$$

So the original 2-D integration in u and v has been reduced to a 1-D integral in ρ, and the singularity has been removed. The integration in ρ can easily be computed with a 1-D Gauss-Legendre quadrature rule.

Unlike other integration methods designed to deal with the spatial integration, the polar method is optimized to integrate in space-time. This leads to the calculation of much more efficient and accurate potential calculations.

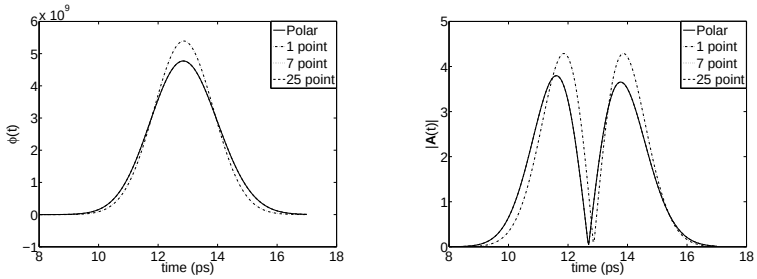

(a) (b)

Figure 4: *Potentials from a negative Gaussian pulse with standard deviation $\sigma = 5ps$. The source triangle has vertices $(0,0,0)$, $(1,0,0)$, and $(0,1,0)$, and the observation point is $(2,2,0)$, where all positions are measured in millimeters, (a) $\phi(t)$, (b) $|\mathbf{A}(t)|$. Because the triangles are electrically small, all methods except 1-point Gaussian are sufficient to predict the shape of the potentials.*

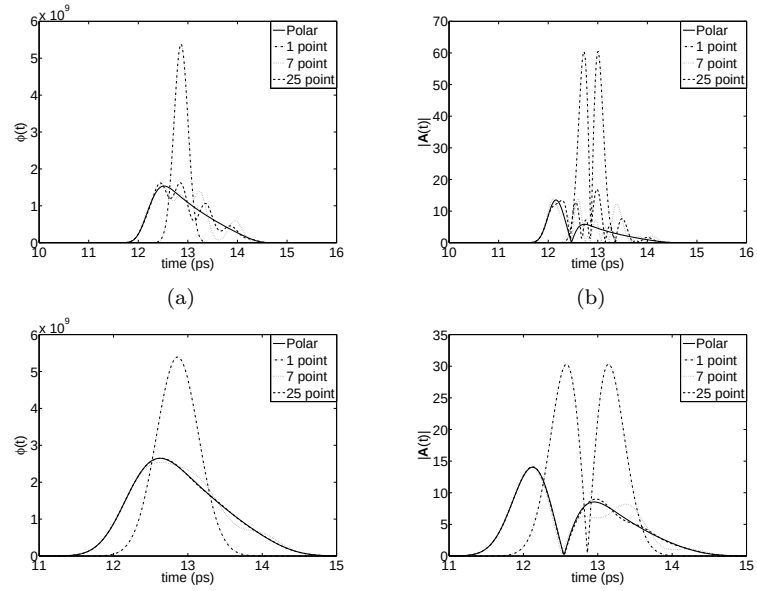

(a) (b)

(c) (d)

Figure 5: *Potentials from a negative Gaussian pulse with standard deviation σ. The source triangle has vertices $(0,0,0)$, $(1,0,0)$, and $(0,1,0)$, and the observation point is $(2,2,0)$, where all positions are measured in millimeters. (a) $\phi(t)$: $\sigma = 0.1ps$, (b) $|\mathbf{A}(t)|$: $\sigma = 0.1ps$, (c) $\phi(t)$: $\sigma = 0.2ps$, (d) $|\mathbf{A}(t)|$: $\sigma = 0.2ps$. In (c) and (d), the 25-point line is nearly indistinguishable from the polar integration result.*

2.3 Numerical Results

In this section, the time domain polar integration scheme is used to compute the electric scalar and magnetic vector potentials at a point due to a half-RWG function on a single triangle. The method is compared to 2-D Gaussian quadrature using 1, 7, and 25 points with singularity extraction. In all cases, the source triangle has vertices $(0, 0, 0)$, $(1, 0, 0)$, and $(0, 1, 0)$, where the units are in millimeters.

In the first example, Figure 4, the potentials are compared for a relatively broad Gaussian pulse, where $\sigma = 1ps$. Other than 1-point Gaussian quadrature, all methods accurately predict the shape of the curve and no spurious high-frequency components are present. When elements are electrically small, the polar method is not needed.

Figure 5 shows the potentials produced by negative Gaussian pulses with mean standard deviation σ. In Figures 5a and 5b, $\sigma = 0.1ps$. Figures 5c and 5d show the results from a wider pulse where $\sigma = 0.2ps$. As can be seen in the figures, when the $P(t)$ pulse is narrow, the Gaussian schemes do not accurately integrate (21). However, when the $P(t)$ pulse is wide, higher-order Gaussian schemes work very well, to the extent that the 25-point Gaussian curve is nearly indistinguishable from the polar integration curve in Figures 5c and 5d. The reason for this is that Gaussian quadrature is designed to integrate slowly-varying, polynomial functions. When the integrand exhibits rapid variations, an extremely high-order Gaussian scheme is required to integrate accurately.

The most critical application of the polar integration scheme is for singular or very-near singular integrations, shown in Figure 6, where it is compared to Gaussian quadrature with singularity extraction. As can be seen in Figures 6c and 6d, the Gaussian quadrature schemes do not show adequate convergence, even when the $P(t)$ pulse is wide. In all cases the Gaussian scheme gives undue weight to the response at the centroid, giving a maximum where the input signal is a maximum, instead of when nearby responses have propagated to the observer.

Finally, Figure 7 shows the fall of a negative square pulse, where the rise and fall are modeled with half-sinc functions. Convergence can be seen as higher-order Gaussian schemes are used, approaching the results from polar integration. The small negative error seen in the 1-point line of Figure 7c results from inaccurate quadrature of the non-singular part of the integral. This error decreases as the Gaussian order increases. Figures 7c and 7d in particular show more accurate integration schemes picking up contributions closer to the triangle edge. The waveform is also much more smooth than the Gaussian quadrature schemes.

It is important to note that in each case above, the area under the group of curves is the same (within 2%). However, the shape of the potential curves is of critical importance. Integrating efficiently in delay places interactions appropriately in the time history, and removes spurious high frequencies from the potentials. Figure 4 shows that Gaussian integration is suitable for electrically small source elements, producing results identical to polar integration. However, when the interactions become more explicit, polar integration method is

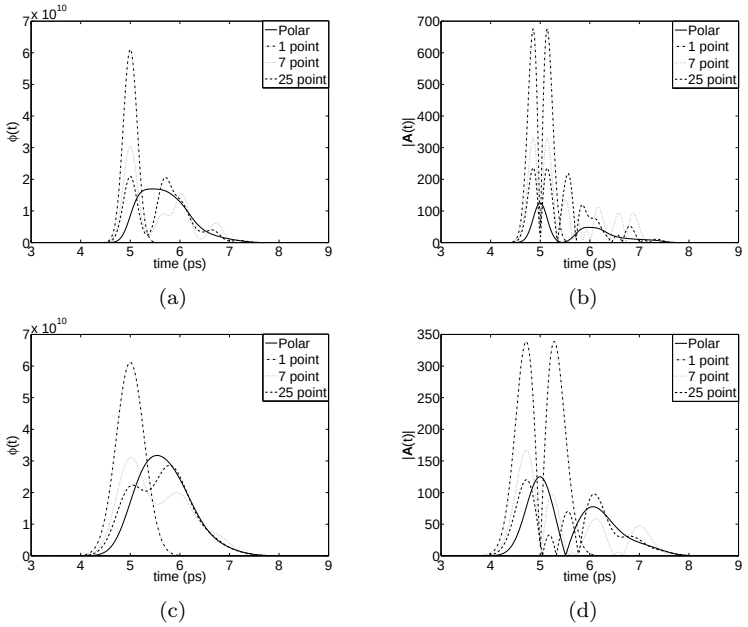

Figure 6: *Potentials from a negative Gaussian pulse with standard deviation σ. The figure compares polar integration to Gaussian quadrature with singularity extraction. The source triangle has vertices* $(0,0,0)$, $(1,0,0)$, *and* $(0,1,0)$, *with the observation point at* $(\frac{1}{3},\frac{1}{3},0)$ *(the triangle centroid), where all distances are measured in millimeters. (a)* $\phi(t)$*:* $\sigma = 0.1ps$*, (b)* $|\mathbf{A}(t)|$*:* $\sigma = 0.1ps$*, (c)* $\phi(t)$*:* $\sigma = 0.2ps$*, (d)* $|\mathbf{A}(t)|$*:* $\sigma = 0.2ps$*.*

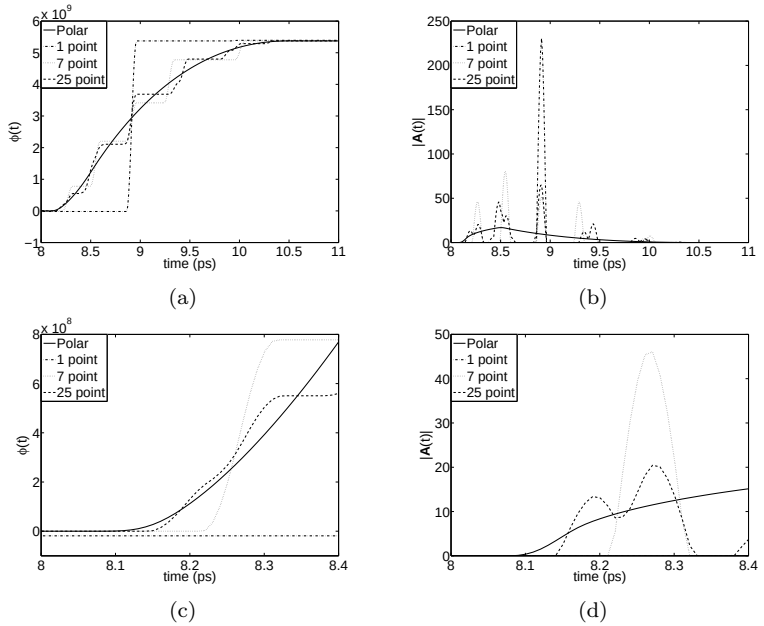

Figure 7: *Potentials from a 9ps negative square pulse with 0.1ps rise/fall time, using various quadrature schemes. The source triangle has vertices* $(0,0,0)$*,* $(1,0,0)$*, and* $(0,1,0)$*, and the observation point is* $(2,2,0)$*, where all distances are measured in millimeters. (a)* $\phi(t)$*, (b)* $|\mathbf{A}(t)|$*, (c) zooming in on front of pulse for* $\phi(t)$*, (d) zooming in on front of pulse for* $|\mathbf{A}(t)|$

.

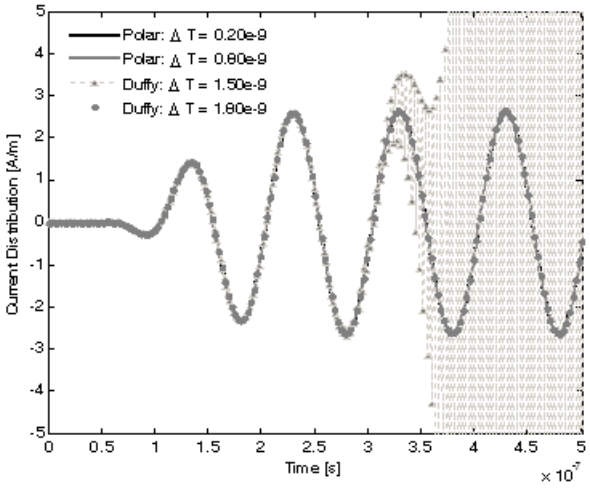

Figure 8: *This figure shows an example run on a unit cube. Polar quadrature enables stability at a much smaller time step than Duffy's method.*

required to capture the shape of the potential interactions.

Figure 8 shows simulations run on a 1-meter cube, modeled with 48 unknowns, using polar quadrature and Duffy's method. Because it is optimized to compute the shape of the potentials, polar integration provides stability at a much smaller time step than Duffy's method.

2.4 Conclusions

In summary, polar integration is necessary for cases where the temporal function exhibits rapid variations (with respect to propagation time across the source triangle), and for singular (or nearly-singular) observation points. The polar scheme is especially attractive because the integrand is rendered non-singular, and the integration becomes one dimensional. In addition, polar integration is equally applicable to all interactions, near and far. Finally, because the numerical integration is one dimensional, it is easy to adaptively integrate the potentials to arbitrary accuracy. Experiments performed at LLNL showed polar integration to greatly increase the stability of electromagnetic TDIEs, beyond any other integration method used.

3 Multigrid Methods

During a preliminary meeting about the fast solver in July of 2005, a method was proposed for speeding up the time history calculation by lumping distant interactions together on a coarser mesh. The underlying idea is that distant

interactions contribute little to the solution, so approximating them will not adversely affect the final solution. The solution method consists of the following steps:

- Create several meshes of varying detail.
- Solve the problem on the mesh.
- As interactions occur further back in the time history, project several matrices from the fine mesh to a coarser mesh. The coarser mesh represents a reduction of unknowns in both time and space, and is used only in the time history calculation.
- Repeat the coarsening as the interactions move back in the history.

This is related to the multigrid method pioneered by Brandt [13] as a method for the iterative solution of finite element problems. It was later adapted to the method of moments for asymptotically smooth kernels (static problems in electromagnetics) [25]. The method has seen limited use in the method of moments, where it is generally referred to as the multilevel method. Some examples can be found in [26–28]. The most relevant work found in the literature is [28] where the multilevel method is applied to 2-D frequency domain electromagnetics as a preconditioner to an iterative solver. The method saw some success, but was never applied to 3-D. To our knowledge, the multilevel method has never been applied to the time domain in either boundary or volume methods.

Mathematically, the proposed method takes the following form: The original TDIE equation is described as

$$\overline{\overline{Z}}_0 \cdot \overline{J}_t = \overline{V} - \sum_{n=1}^{N_h} \overline{\overline{Z}}_n \cdot \overline{J}_{t-n} \tag{22}$$

where $\overline{\overline{Z}}_n$ describes the scattered electric field generated on the mesh at the present time due to currents that occurred n time steps ago, $\overline{J}_i$ is the current at time step i, N_h is the number of time history matrices, and $\overline{V}$ is the tested electric field at the present time step. The goal of the method is to transform (22) into (23):

$$\overline{\overline{Z}}_0 \cdot \overline{J}_t = \overline{V} - \sum_{n=1}^{N^1} \overline{\overline{Z}}_n \cdot \overline{J}_{t-n} - \sum_{N^1+1=1}^{N^2} \overline{\overline{Z}}^1_n \cdot \overline{J}^1_{t-n} - \sum_{N^2+1=1}^{N^3_h} \overline{\overline{Z}}^2_n \cdot \overline{J}^2_{t-n} \tag{23}$$

where the superscript indicates the mesh coarseness level. The higher the superscript, the coarser the mesh. In general, as the TDIE looks further into the time history, the coarser the mesh and time step used to represent the currents. Equation 23 represents a problem where only 3 levels are used. The unknowns

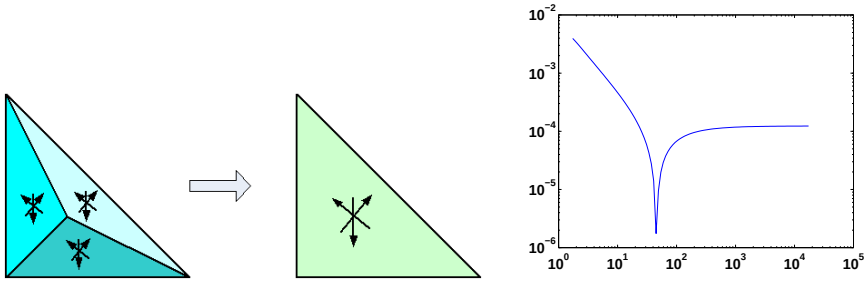

(a) (b)

Figure 9: *Projection of basis functions from three triangles to a single triangle. (a) shows the spatial operation, (b) shows the error as a function of radius from the triangle centroid for a triangle with vertices (0,0,0), (0,1,0), and (1,0,0).*

are related by some matrix, $\overline{\overline{P}}$, where $\overline{J}^{k+1} = \overline{\overline{P}}_k^{k+1} \cdot \overline{J}^k$. The goal of this research was to find a suitable $\overline{\overline{P}}_k^{k+1}$ that could accurately and efficiently project the unknowns from the fine mesh/time to the coarse mesh/time.

Because this method was untried in the literature, and due to the fickle nature of the time domain electric field integral equation, this solution strategy carried some risk. In particular, it carried two assumptions:

- using an approximate solution for distant interactions would not greatly affect solution accuracy
- a mapping could be found to accurately project the fine solution onto the coarse mesh in $O(N)$ time

The rest of this report examines the validity of these assumptions. The approach taken was to attack spatial and temporal projection separately, then combine the two projection techniques.

3.1 Spatial Projection

The first objective was spatial projection, which is a well-known area. The method we chose was far field point matching, where E_x, E_y, and E_z are matched at testing points in space between original and projected currents. The underlying idea is that, given a set of basis functions, one can match the fields they produce at a set of points in space through the relation

$$\overline{\overline{P}}^{\,c} \cdot \overline{J}^{\,c} = \overline{\overline{P}}^{\,f} \cdot \overline{J}^{\,f}, \tag{24}$$

where the vectors $\overline{J}^{\,c}$ and $\overline{J}^{\,f}$ are the weights of the coarse and fine basis functions. The matrix entry P_{ij} is the field at the $i^{\,th}$ point in space due to the $j^{\,th}$ basis function. The f and c superscripts represent the fine and coarse

projections, respectively. In actuality, there are $3N_s$ rows of P^c and P^f, where N_s is the number of spatial testing points, one for each Cartesian component of the electric field. The projection matrix P from the fine to the coarse basis functions can then be computed as

$$\overline{\overline{P}} = \overline{\overline{P}}^{c+} \cdot \overline{\overline{P}}^{f} \tag{25}$$

where $\overline{\overline{P}}^{c+}$ is the Moore-Penrose pseudoinverse of $\overline{\overline{P}}^{c}$. If there were no temporal aspects to consider, then the projection would be as simple as computing $\overline{J}^{c}$ for each time step as

$$\overline{J}^{c} = \overline{\overline{P}} \cdot \overline{J}^{f}. \tag{26}$$

Figure 9 shows the idea of the spatial projection process and the error in projection as a function of radius.

3.2 Temporal Projection

As the mesh is now coarser than the original, the original time step is overdescriptive. Indeed, because a coarse mesh element is likely large enough to cover the propagation distance of several fine time steps, a temporal projection scheme is also needed.

This projection method essentially acts as a low pass filter and downsampler on the unknowns in the time history. To keep the projection method computationally inexpensive, it must operate locally on the time history, looking neither forward nor backward in the time history. It is recognized that there was only one degree of freedom to use in this projection: the weight of the coarse mesh basis function. The most logical projection method in this case is to enforce that the area under the curve of the coarse time sequence is the same as the area under the curve of the fine sequence. Mathematically, this is expressed as

$$w_c = \frac{\Delta t_f}{\Delta t_c} \sum w_f, \tag{27}$$

where w_c and w_f are the weights of the basis functions and Δt_c and Δt_f are the time steps. This method achieved decent results, as shown in Figure 10. [5].

While this method does a good job of locally computing a low pass filter operation, the question remains as to whether or not the filtered sequence accurately represents the solution. The projected field shows only 75% correlation with the original sequence, and this may not be good enough to support accurate solution. At the request of the ACE lab, an experiment was performed at LLNL where a digital low pass filter was applied to the time history (while keeping the number of samples the same). This accurately models the temporal projection without adding the complication of the spatial projection. The filter was applied starting at 25%, 50%, and 75% of the time history for the problem of a dipole radiating into free space. The results are shown in Figure 11. As can be seen, the filtered solution only shows agreement with the unfiltered solution when applied to the final 25% of the time history (starting at 75% through the

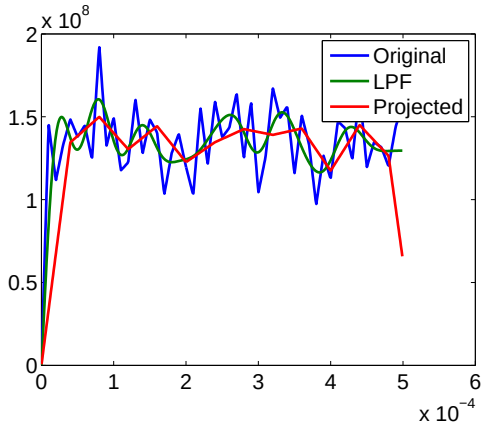

Figure 10: *Magnitude of the E field from randomly generated weights, superimposed with the low-pass filter of the time sequence and the projected sequence. As can be seen, the projection method does a fair job of approximating a low pass filter.*

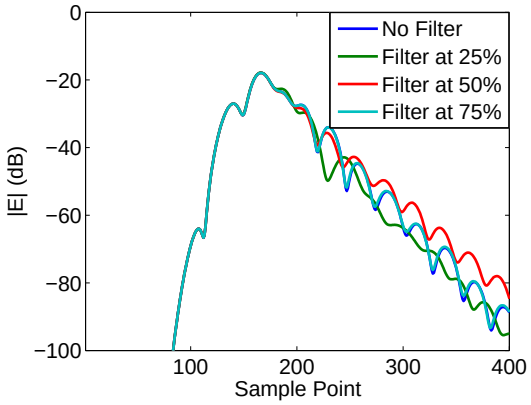

Figure 11: *Results of a low pass filter test on the hybrid. A low pass filter was applied at 25%, 50%, and 75% of the time history for a dipole radiating into free space. The solutions are compared against the unfiltered solution, which has shown excellent results compared to the analytical solution.*

history). The error in the other two trials begins as soon as the time history reaches the filtered section. Therefore, the projection method can only reduce the problem by a maximum of 25% without damaging the result.

3.3 Combined Spatio-Temporal Projection

This step involves combining the spatial and temporal projections, resulting in a single projection from the fine mesh to the coarse mesh. The goal was a single projection from the fine mesh to the coarse mesh of the form

$$\overline{\overline{Z}}^{\,c} = \overline{\overline{P}} \cdot \overline{\overline{Z}}^{\,f} \tag{28}$$

where $\overline{\overline{Z}}^{\,c}$ and $\overline{\overline{Z}}^{\,f}$ are the coarse and fine time history matrices, respectively, and $\overline{\overline{P}}$ is the projection matrix. A complication is added in that, from different angles of observation, the elements of the fine mesh would project onto different time steps of the coarse mesh. This requires angle dependent projection, greatly increasing the complexity and computational cost of the solver. Due to this and the limitations shown in Section 3.2, the benefits of this solution method further were deemed minimal. Hence, this approach was not pursued further.

4 Conclusions

This work contributed further to our understanding of the time domain integral equations. The work shown in Section 2 shows that accurate integration of the retarded potentials plays a significant role in the stability of the electric field integral equation. The accuracy of the polar integration method provides a solution to this problem. Additionally, work was performed to investigate the idea that the phase of distant interactions can be dealt with in an approximate manner. The research showed that this is only valid for the final 25% of the time history. Earlier interactions must be dealt with in a more exacting manner.

5 Publications

The following is a list of publications that resulted from this research:

- J. Pingenot, S. Chakraborty, and V. Jandhyala, "Polar integration for exact space-time quadrature in time-domain Integral equations," IEEE Transactions on Antennas and Propagation, v. 54, n. 10, 2006.
- J. Pingenot, C. Yang, V. Jandhyala, B. Fasenfest, R. Rieben, D. White, R. Sharpe, M. Stowell, N. Madsen, and J.D. Rockway, "A generalized TDIE framework for arbitrary time basis functions," 2005 IEEE Antennas and Propagation Society International Symposium, Washington, D.C., July 3-8, 2005, v. 3B, p. 443-446.

- J. Pingenot, C. Yang, V. Jandhyala, N. Champagne, D. White, M. Stowell, R. Rieben, and R. Sharpe, "Surface based differential forms," 2005 IEEE/ACES International Conference on Wireless Communications and Applied Computational Electromagnetics, Honolulu, HI, April 3-7, 2005, p. 694-697.

References

[1] C. Solloway and M. Sarto, "On the use of a hybrid IE/FDTD method for the analysis of electromagnetic scattering and coupling problems," in *IEEE International Symposium on Electromagnetic Compatibility.*

[2] D. Jiao, A. A. Ergin, B. Shanker, E. Michielssen, and J.-M. Jin, "A fast higher-order time-domain finite element-boundary integral method for 3-d electromagnetic scattering analysis," *IEEE Trans. Antennas Propagat.*, vol. 50, no. 9, pp. 1192–1202, Sept. 2002.

[3] M. Sarto and A. Scarlatti, "Efficient numerical calculation of integral equations-boundary conditions for the finite-difference time-domain method," *IEEE Trans. Magn.*

[4] B. Shanker, M. Lu, A. A. Ergin, and E. Michielssen, "Plane-wave time-domain accelerated radiation boundary kernels for FDTD analysis of 3-D electromagnetic phenomena," *IEEE Trans. Antennas Propagat.*

[5] B. Shanker, A. A. Ergin, M. Lu, and E. Michielssen, "Fast analysis of transient electromagnetic scattering phenomena using the multilevel plane wave time domain algorithm," *IEEE Trans. Antennas Propagat.*

[6] K. Aygün, M. Lu, M. Lu, A. E. Yilmaz, and E. Michielssen, "A parallel PWTD accelerated time marching scheme for analysis of EMC/EMI problems," in *IEEE International Symposium on Electromagnetic Compatibility (EMC).*

[7] N. Liu, M. Lu, B. Shanker, and E. Michielssen, "The parallel plane wave time domain algorithm-accelerated marching on in time solvers for large-scale electromagnetic scattering problems," in *IEEE Antennas and Propagation Society Symposium.*

[8] A. E. Yilmaz, J.-M. Jin, and E. Michielssen, "A hierarchical FFT algorithm (HIL-FFT) for the fast analysis of transient electromagnetic scattering phenomena," *IEEE Trans. Antennas Propagat.*, vol. 50, no. 7, pp. 971–982, July 2002.

[9] ——, "Time domain adaptive integral method for surface integral equations," *IEEE Trans. Antennas Propagat.*, vol. 52, no. 10, pp. 2692–2708, Oct. 2004.

[10] A. E. Yilmaz, A. Z. Lou, E. Michielssen, and J.-M. Jin, "A parallel time-domain adaptive integral method-accelerated single-boundary finite element-boundary integral solver," in *2006 IEEE Antennas and Propagation Society International Symposium*, 2006, p. 297.

[11] A. E. Yilmaz, J.-M. Jin, and E. Michielssen, "A parallel FFT accelerated transient field-circuit simulator," *IEEE Trans. Microwave Theory Tech.*, vol. 53, no. 9, pp. 2851–2865, Sept. 2005.

[12] D. Gope and V. Jandhyala, "Oct-tree based multilevel low-rank decomposition algorithm for rapid 3D parasitic extraction," *IEEE Trans. Computer-Aided Design*, vol. 23, no. 11, pp. 1575–1580, Nov. 2004.

[13] A. Brandt, "Multi-level adaptive solutions to boundary-value problems," *Mathematics of Computation*, vol. 31, no. 138, pp. 333–390, Apr. 1977.

[14] Y.-S. Chung, T. K. Sarkar, B. H. Jung, M. Salazar-Palma, Z. Ji, S. Jang, and K. Kim, "Solution of time domain electric field integral equation using the Laguerre polynomials," *IEEE Trans. Antennas Propagat.*, vol. 52, no. 9, pp. 2319–2328, Sept. 2004.

[15] D. S. Weile, G. Pisharody, N.-W. Chen, B. Shanker, and E. Michielssen, "A novel scheme for the solution of the time-domain integral equations of electromagnetics," *IEEE Trans. Antennas Propagat.*, vol. 52, no. 1, pp. 283–295, Jan. 2004.

[16] G. Manara, A. Monorchio, and R. Reggiannini, "A space-time discretization criterion for a stable time-marching solution of the electric field integral equation," *IEEE Trans. Antennas Propagat.*, vol. 45, no. 3, pp. 527–532, Mar. 1997.

[17] M. J. Bluck and S. P. Walker, "Time-domain BIE analysis of large three-dimensional electromagnetic scattering problems," *IEEE Trans. Antennas Propagat.*, vol. 45, no. 5, pp. 894–901, May 1997.

[18] M. Abramowitz and I. Stegun, Eds., *Handbook of Mathematical Functions*. Dover Publications, 1977.

[19] D. R. Wilton, S. M. Rao, and A. W. Glisson, "Electromagnetic scattering by arbitrary surfaces," Rome Air Development Center, Griffiss AFB, NY, Tech. Rep. RADC-TR-79-325, Mar. 1980.

[20] M. G. Duffy, "Quadrature over a pyramid or cube of integrands with a singularity at a vertex," *SIAM Journal of Numerical Analysis*, vol. 19, no. 6, pp. 1260–1262, Dec. 1982.

[21] R. A. Wildman and D. S. Weile, "Two-dimensional transverse-magnetic time-domain scattering using the Nyström method and bandlimited extrapolation," *IEEE Trans. Antennas Propagat.*, vol. 53, no. 7, pp. 2259–2266, July 2005.

[22] M. A. Khayat and D. R. Wilton, "Numerical evaluation of singular and near-singular potential integrals," *IEEE Trans. Antennas Propagat.*, vol. 53, no. 10, pp. 3180–3190, Oct. 2005.

[23] M. J. Bluck, M. D. Pocock, and S. P. Walker, "An accurate method for the calculation of singular integrals arising in time-domain integral equation analysis of electromagnetic scattering," *IEEE Trans. Antennas Propagat.*, vol. 45, no. 12, pp. 1793–1797, Dec. 1997.

[24] S. Chakraborty and V. Jandhyala, "Evaluation of Green's function integrals in conducting media," *IEEE Trans. Antennas Propagat.*, vol. 52, no. 12, pp. 3357–3363, Dec. 2004.

[25] A. Brandt and C. H. Venner, "Multilevel evaluation of integral transforms with asymptotically smooth kernels," *SIAM Journal of Scientific Computation*, vol. 19, no. 2, pp. 468–492, Mar. 1998.

[26] P. W. Hemker and H. Schippersa, "Multiple grid methods for the solution of Fredholm integral equations of the second kind," *Mathematics of Computation*, vol. 36, no. 153, Jan. 1981.

[27] J. Mandel, "On multilevel iterative methods for integral equations of the second kind and related problems," *Numerical Mathematics*, vol. 46, pp. 147–157, 1985.

[28] K. Kalbasi and K. R. Demarest, "Multilevel formulation of the method of moments," *IEEE Trans. Antennas Propagat.*, vol. 41, no. 5, pp. 589–599, May 1993.